Tunable electron counting statistics in a quantum dot at thermal equilibrium

X. C. Zhang,[1] G. Mazzeo,[2] A. Brataas,[3] M. Xiao,[1] E. Yablonovitch,[4] and H. W. Jiang[1]

[1]*Department of Physics and Astronomy, University of California at Los Angeles,*
405 Hilgard Avenue, Los Angeles, California 90095, USA

[2]*Department of Electrical Engineering, University of California at Los Angeles, Los Angeles, California 90095, USA*

[3]*Department of Physics, Norwegian University of Science and Technology, NO-7491 Trondheim, Norway*

[4]*Department of Electrical Engineering, University of California at Berkley, Berkley, California 94720, USA*

Tunneling of individual electrons into and out of a GaAs quantum dot is measured in real time by an adjacent charge detector. By controllably increasing the tunneling rate at thermal equilibrium, the full-counting statistics of these tunneling events shows a sub- to super-Poissonian transition, accompanied by a sign reversal of its third statistical moment. These anomalies are believed to be caused by electron tunneling through the singlet-triplet states of an elongated double dot, confirmed by a self-consistent Poisson-Schrödinger wave-function calculation.

I. INTRODUCTION

Single-photon counting statistics is a frequently used technique to probe the internal structure and entanglement in quantum optical systems.[1] Very recently, experimental works[2–5] of single-electron counting statistics have emerged toward the goal of making such quantum measurements in semiconductor quantum dots (QDs). These works were both inspired by the development of a theoretical foundation of full-counting statistics (FCS) (Refs. 6 and 7) and facilitated by the experimental implementation of on-chip charge detectors[8–10] with a single-electron sensitivity. The charge fluctuations, manifested as discrete steps of detector current, have the characteristic signature of the random telegraph signal (RTS), commonly observed in mesoscopic systems. The FCS (i.e., the statistical moments) of the RTS can provide additional information of quantum systems beyond the conventional dc transport study.[11] For example, Coulomb correlations cannot only suppress the second moment (i.e., the shot noise or the standard deviation of the distribution function) and third moment (i.e., the asymmetry or the skewness) in the nonequilibrium condition when a single QD is voltage biased[5] but also dictate the single-electron current statistics flow pattern in a double QD.[3]

In this work we performed an experiment in a QD in the few-electron regime. In contrast to earlier work, we focus on the spontaneous tunneling events between the dot and the reservoir, via a single barrier, at thermal equilibrium. We have observed anomalous behavior in the FCS when the confinement potential of the QD is biased into an elongated shape. As we controllably increase the electron-tunneling rate, the second moment shows a sub- to super-Poissonian transition. This excessively large noise is also accompanied by a large negative third moment. We used the anomalous results to explore the internal level structure of the QD based on the FCS.[4]

II. QD FABRICATION AND MEASUREMENT TECHNIQUES

The QDs were fabricated from a molecular-beam epitaxy (MBE) grown GaAs/AlGaAs heterostructure containing a two-dimensional electron gas (2DEG) 100 nm below the surface with a density of 2.8×10^{11} cm^{-2} and a mobility of 1.78×10^5 cm$^2 \cdot$V$^{-1} \cdot$s^{-1}. The surface gates in Fig. 1(c) share a similar design with Refs. 9 and 12, consisting of 5/30 nm Cr/Au film defined by electron-beam lithography and lift-off process. The electrical contacts to the source and drain reservoir are provided by annealing the Ni/AuGe film evaporated on the contact pads patterned by wet chemical etching. The charge state of the QD, defined by gates T, M, P, and R can be probed by the neighboring one-dimensional (1D) channel formed by gates R and Q. The conductance of the 1D channel switches between two discrete values when an extra electron tunnels into or out of the QD, as shown in Fig. 1(b). The plunger gate P is used for fine tuning the QD potential. All the measurements were performed in a He^3 cryostat with a base temperature of 0.34 K. The electron temperature was 0.5 K deduced from the RTS data as shown
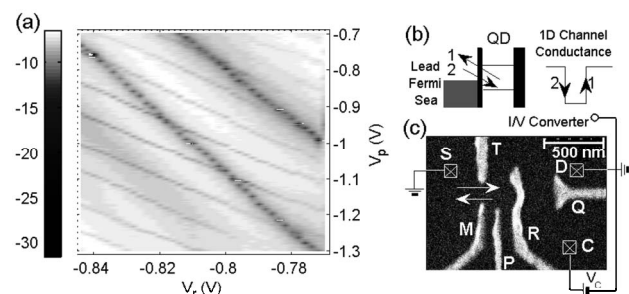

FIG. 1. (a) Grayscale plot of the transconductance dI/dV_M (in arbitrary units) of the 1D read-out channel versus V_R and V_P. The modulation signal on gate M is a 3.8 mV/83.27 Hz sine wave. The lines correspond to abrupt changes in the channel conductance when single electrons enter and leave the QD, as shown in (b). (c) is the scanning electron microscope (SEM) picture of the device and the measurement configuration. The crossed squares denote the Ohmic contacts. During measurements the S and D contacts were grounded. A voltage V_C biased 1D channel formed by gates R and Q was used to sense the electron-tunneling events (denoted by double arrows) through the one-barrier-open QD confined by T, M, P, and R gates.
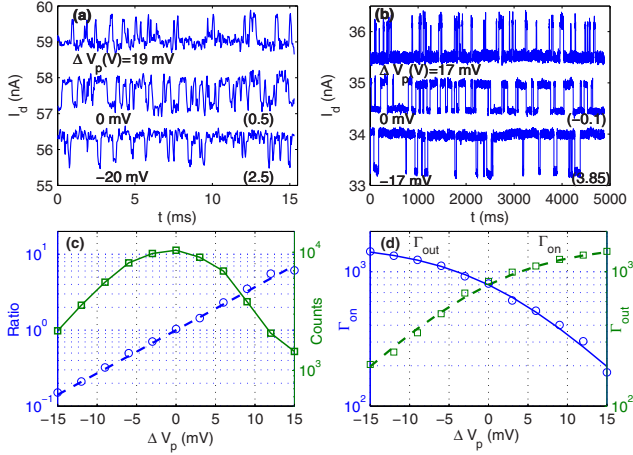
FIG. 2. (Color online) One (a) fast and (b) slow RTS trace, and their evolution with V_P, represent the real-time electron tunneling through the last two QD states. The number in brackets is the offset along the y axis. (c) The ratio (circles associated with the left y axis) of average time of RTS in the high and low current states, and the total number of transitions (squares associated with the right y axis) are plotted against the unbalanced plunger gate voltage ΔV_p. The dashed line is the exponential fit according to $r=\exp[\alpha e(V_p-V_{P0})/kT]$. (d) The experimental tunneling rates, Γ_{in} (squares) and Γ_{out} (circles), are plotted as a function of ΔV_p. Curves are the fit according to Eq. (1).

below. During measurements the QD was tuned to have only its left barrier weakly coupled to the 2DEG reservoir. The 1D channel was tuned near $2h/e^2 \approx 52$ KΩ with a dc bias of 0.8 mV. Further decreasing the channel bias does not alter the RTS statistics noticeably, which implies that the heating effect is negligible. The recorded RTS typically has current switchings 5% of its average current and a signal-to-noise ratio of about 5:1.

III. RTS AND ELECTRON COUNTING STATISTICS

Figure 1(a) shows the grayscale plot of the transconductance of the readout channel, dI/dV_M, versus gate voltage V_R and V_P. This modulation technique can reveal QD states, which are otherwise invisible in the QD average current measurement due to the rather opaque tunneling barrier.[13] Each gray line in this plot represents the evolution of an individual QD state with V_R and V_P. The QD is in the few-electron region, evidenced by the uneven spacing between the gray lines in the left-bottom portion of Fig. 1(a).

Monitoring the 1D channel current in real time reveals one fast and one slow RTS, which appear successively in close proximity to the two bottom gray lines of Fig. 1(a). Both the fast and slow RTS, shown in Figs. 2(a) and 2(b), respectively, exhibit a clear evolution with V_P. The observed shortest RTS duration indicates that the bandwidth of the measurement system is about 35 KHz, which is comparable with Refs. 5 and 8.

The reconstructed RTS, following the algorithm in Ref. 10, was used to extract the ratio of the average time that RTS stays in its two discrete states. The logarithm of the ratio,
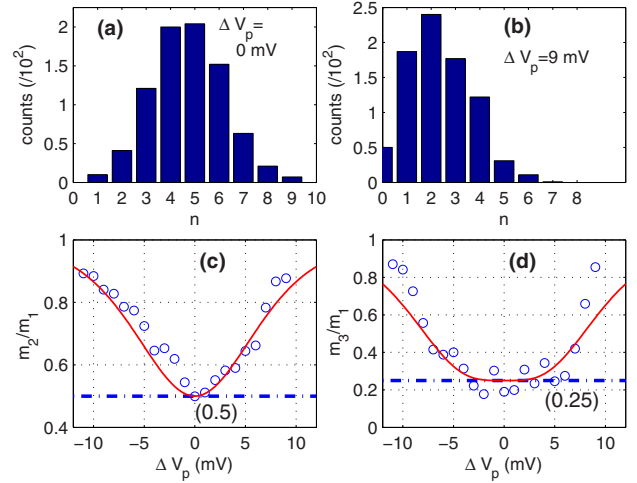

FIG. 3. (Color online) The probability distribution function of the number of electrons tunneling through the QD within a finite length of time, t_0, at the (a) balanced condition of $\Delta V_p=0$ and (b) unbalanced conditions. (c) $\frac{m_2}{m_1}$ and (d) $\frac{m_3}{m_1}$ are plotted as a function of ΔV_p. Red (dark gray) lines indicate the theoretical values according to Eq. (4); blue (dark gray) dashed lines indicate $\frac{m_2}{m_1}=0.5$ and $\frac{m_2}{m_1}=0.25$ at the balance point.

$\log(r)$, is found to exhibit a linear relationship with V_p, as shown in Fig. 2(c), and the total switchings in the RTS, N, shows a peak value at $r=1$. From the detailed balance condition,[14] $r=\exp[(E_d-E_f)/kT]$, where E_d and E_f are the energy level of the QD and Fermi level of the lead, respectively. Thus $E_d-E_f=\alpha e\Delta V_p=\alpha e(V_p-V_{P0})$, where α is the arm factor, V_{P0} is the balance point where $r=1$, and E_d is exactly aligned with E_f. The linear fit in Fig. 2(c) gives an effective electron temperature of 0.5 K using $\alpha=0.011$ extracted from the QD Coulomb diamond diagram.

The rate of electron tunneling into (out of) the QD can be derived from RTS traces according to $\Gamma_{in(out)}^{-1}=2\cdot t_{H(L)}/N$, where t_H and t_L are the total duration of the two discrete RTS states. The obtained $\Gamma_{in(out)}$ versus ΔV_P is shown in Fig. 2(d). The relation between the effective tunneling rate and the dot-lead coupling strength Γ is

$$\Gamma_{in/out} = \Gamma \cdot f(\pm \Delta E/kT), \qquad (1)$$

where $\Delta E=E_f-E_d$ and $f(\Delta E/kT)$ is the Fermi-Dirac distribution.[4] In Fig. 2(d), the theoretical curve formulated by Eq. (1) shows excellent agreement with the experimental data. An increasing V_P will lower the electrochemical potential of the QD, and Γ_{in} (Γ_{out}) will increase (decrease) accordingly. At the balance point, $\Gamma_{in}=\Gamma_{out}$, corresponding to $r=1$ and the maximum N in Fig. 2(c).

Two consecutive up and down steps in a RTS trace constitute one cycle of an electron entering and leaving the QD. For a RTS trace with a total time length T, by counting the electrons within its individual time division t_0, the statistics of the number of electrons tunneling through the QD can be constructed.[5] The resultant probability distribution functions at different V_P's are plotted in Figs. 3(a) and 3(b) for the fast

RTS at $\Gamma = 100$ Hz. Each RTS trace contains about 10 000 transitions so that the obtained statistics are insensitive to the RTS length.

The distribution function at the balance point in Fig. 3(a) shows a larger center (average) value $\langle n \rangle$ and is more symmetric and broader than those at unbalanced conditions in Fig. 3(b). The distribution function can be understood in the framework of the FCS. We treat the problem as a QD at thermal equilibrium with only its left tunneling barrier weakly coupled to the thermal reservoir. The master equation that describes the time evolution of the system is

$$\frac{\partial}{\partial t}|p,t\rangle = -\hat{L}|p,t\rangle, \quad |p,t\rangle = \begin{pmatrix} p_1 \\ p_2 \end{pmatrix}, \tag{2}$$

where p_1 and p_2 are the occupation probabilities of one- and two-electron states, respectively.[7] As originally proposed in Ref. 7, electrons tunneling out of the QD can be counted by adding a counting factor $e^{i\chi}$ to one of the off-diagonal elements of the matrix L, which represents the possible transition probability between the states,

$$\begin{pmatrix} \Gamma_{in} & -\Gamma_{out} \cdot e^{i\chi} \\ -\Gamma_{in} & \Gamma_{out} \end{pmatrix}. \tag{3}$$

The central moments, m_n, can be obtained from the lowest eigenvalue $\lambda_0(\chi)$ of the matrix: $m_n = -(-i\partial_\chi)^n S(\chi)|_{\chi=0}$ and the generating function $S(\chi) = -\lambda_0(\chi)t_0$. The analytical expression for $\frac{m_2}{m_1}$ and $\frac{m_3}{m_1}$ of the system can be derived as

$$\begin{cases} \dfrac{m_2}{m_1} = (1 + \beta^2)/2, \\[2mm] \dfrac{m_3}{m_1} = (1 + 3\beta^4)/4, \end{cases} \tag{4}$$

where $\beta = 2f(\Delta E/kT) - 1$.

The above expressions describe the experimental data quite well, as displayed in Figs. 3(c) and 3(d). The ratios $\frac{m_2}{m_1}$ and $\frac{m_3}{m_1}$ have their minimum values at 0.5 and 0.25 at the balance point, respectively, which clearly deviate from $\frac{m_2}{m_1} = \frac{m_3}{m_1} = 1$ expected for classical Poissonian noise. The suppression is a consequence of the Coulomb blockade effect as one electron can only enter the QD after the previous one exits. This generates a correlation in the electron transport and hence reduces the current fluctuations. The reduction (correlation) is most pronounced at the balance point where there are the most electrons passing through the QD, set by the lower value in Γ_{in} and Γ_{out}, as shown in Figs. 2(c) and 2(d).

The FCS, however, displays an unusual behavior at higher tunneling rate Γ. During the experiment the QD level remains resonant with the Fermi level of the lead, while its left barrier is tuned to become more transparent, as depicted in Fig. 4(c). As we increase Γ, $\frac{m_2}{m_1}$ in Fig. 4(e), which is essentially the quantum noise, deviates from 0.5 and increases to a value, which is even larger than unity, as expected for Poissonian noise. Meanwhile $\frac{m_3}{m_1}$ in Fig. 4(f), a measure of the asymmetry of the distribution function, deviates from 0.25

and reaches a large negative value of about -2.5. This suggests that the noise behavior at the balance point can be tuned from sub-($\frac{m_2}{m_1} < 1$) to super-Poissonian ($\frac{m_2}{m_1} > 1$) solely by the tunneling rate. We believe this peculiar noise behavior is due to the fact that there is more than one orbital state within kT [Fig. 4(b)], i.e., the spin singlet and triplet states of an elongated double QD [Fig. 4(d)] formed at nearly zero plunger gate voltages.[11]

IV. WAVE FUNCTION OF A TWO-ELECTRON QD

To confirm that the QD can be tuned to behave like two weakly coupled dots under low plunger gate voltages, the two-electron wave function has been numerically simulated. The wave function of the electrons confined in a QD can be decomposed as

$$\psi(x, y, z) = \varphi(x, y)\phi(z), \tag{5}$$

where $\varphi(x, y)$ and $\phi(z)$ are the wave-function components in the x-y plane and the z (growth) direction, respectively.

A. 1D self-consistent solution in z-direction

$\phi(z)$ can be obtained by a 1D self-consistent solution of Poisson-Schrödinger solution.[15] Initially assuming no charge at the heterostructure interface, the Schrödinger equation was solved for a step potential formed by the band offset between GaAs and AlGaAs. The ground-state wave function and its eigenenergy can thus be acquired. The charge-density distribution along z-direction can be computed as

$$\rho(z) = e \int_{E_0}^{E_f} D(E)f(E)|\phi(z)|^2 dE, \tag{6}$$

where $D(E)$ is the two-dimensional density of states and E_0 is the energy of the ground subband edge. The attained charge distribution can be substituted into the Poisson equation to solve the potential distribution. This procedure can be repeated until convergence is obtained.

The above calculation was intended to extract information required in the following simulation procedures: (1) the dopant density introduced during the heterostructure growth cannot be used in the definition of the device model since the dopants are only partially ionized at low temperatures. Instead the effective dopant density has been adjusted so that the simulated 2DEG density would match the experimental value. (2) The mismatch between Fermi levels of the gate metal and AlGaAs was extracted by the channel threshold voltage at about -0.4 V instead of using the theoretical work-function values, which are usually not reliable. (3) In the following three-dimensional (3D) Poisson simulation by the finite element method (FEM), due to the limitation of the number of mesh points available in the z direction, the exact distribution of the electron charge in this direction cannot not be reproduced. Instead the charge distribution in the z direction was assumed uniformly distributed in a $z_0 = 20$-nm-thick slab below the heterostructure interface. z_0 is determined by the following relation:
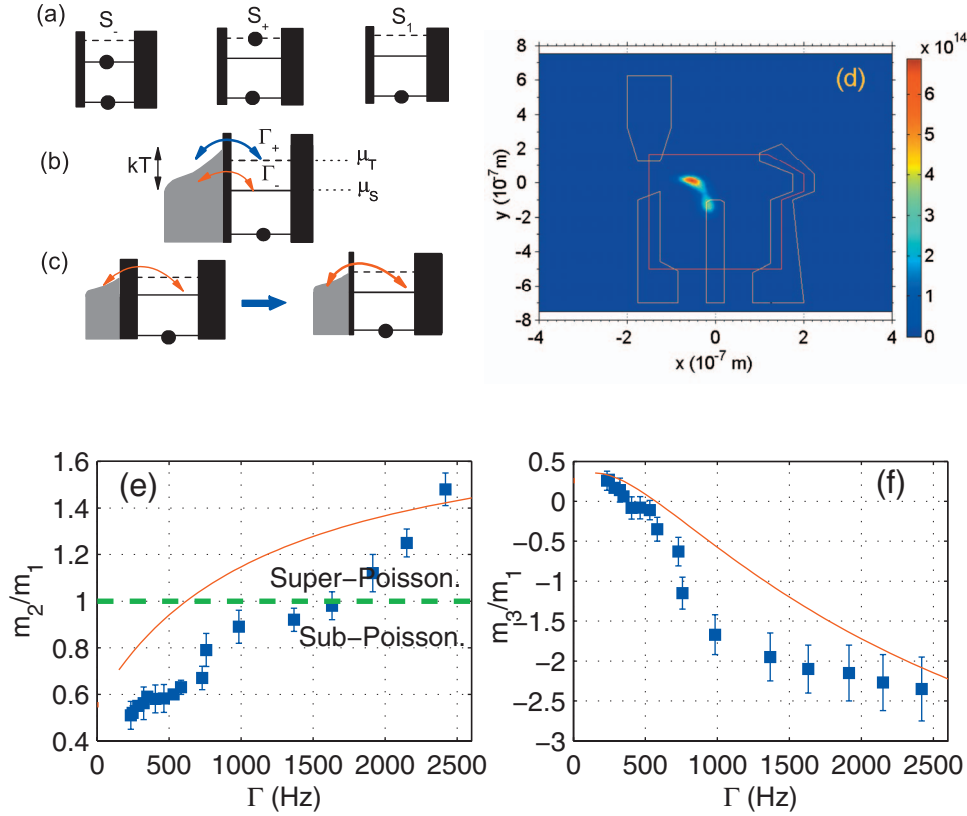
FIG. 4. (Color) (a) QD states in the model. S_- and S_+ are the two-electron singlet and triplet states; S_1 is the one-electron ground state. (b) The model: the QD has only its left barrier weakly open. Electrons can hop on and off states S_+ and S_-, which are within the thermal fluctuation window kT with two drastically different rates Γ^+ and Γ^-. (c) Measurement configuration: the QD level is always aligned with the Fermi level of the lead, while its left barrier becomes more transparent by sweeping V_M and V_P in the opposite direction. (d) The numerically simulated charge-density profile of a two-electron QD at $V_m = -0.85$ V, $V_T = -0.8$ V, $V_R = -1.2$ V, and $V_p = -0.01$ V displays an elongated weakly coupled double QD. (e) $\frac{m_2}{m_1}$ (squares) and (f) $\frac{m_3}{m_1}$ (squares) at the balance point as a function of tunneling rate. The theoretical values for $\frac{m_2}{m_1}$ and $\frac{m_2}{m_1}$ are shown by the curves.

$$\int_0^{z_0} \rho(z)dz \Big/ \int_0^{+\infty} \rho(z)dz = 0.95. \qquad (7)$$

This simplification was proved to be satisfactory and also consistent with the fact that z_0 is much smaller than the size of the QD. (4) Finally the quantum confinement effect was taken into account by shifting the QD energy levels the amount of E_0 from the $\phi(z)$ solution.

B. 3D Poisson problem

The Poisson problem was simulated in a full 3D domain employing the numerical technique of FEM. A 3D domain is required by the structure of the device: even though electrons are laterally confined in a 2D plane, the gate electrodes are located 100 nm above the heterostructure interface. As specified above the electron charge is considered uniformly distributed in the z direction in a 20-nm-thick slab. Inside the quantum dot the charge used in the Poisson problem is extracted from the solution of the 2D Schrödinger equation including the electron-electron interaction, as will be described in the next section.

C. 2D simulation within the QD plane

The charge distribution inside a two-electron QD can be calculated by solving the Schrödinger and Poisson equation self-consistently. The Hamiltonian of the problem can be written as

$$H = \sum_{i=1}^{2} \left[\frac{\hbar^2}{2m^*}\nabla_i^2 + eV(r_i) \right] + H_{ee} + H_{ex}, \qquad (8)$$

where the first term is the kinetic energy and V is the confinement potential defined by the gate voltages and can be numerically extracted from the 3D Poisson simulation. H_{ee} is the Coulomb interactions between electrons. H_{ex} is the exchange interaction due to Pauli exclusion principle and Coulomb interactions. For a weakly coupled two-electron double QD, the confinement potential has a two-minima shape and thus forms two well-separated traps for each electron; it is possible to treat both the Coulomb and exchange interaction as a perturbation to the one-electron Schrödinger equation. However, this is not applicable to our case here since V has only one minimum. Due to the elongated shape of the potential well, the Coulomb repulsion pushes the electrons away

from each other at a considerable distance. This, on one hand, sets the necessity to treat exactly the Coulomb interaction within a self-consistent scheme; on the other hand, the one-electron wave function calculated in this way is centered at a distance large enough to treat the exchange Hamiltonian as a perturbation. Similar situation has also been reported in a wide single-quantum well in which two isolated 2DEG layers are formed due to strong Coulomb repulsion among electrons.[16]

The simulation process is based on one set of coupled nonlinear Schrödinger equations,

$$E_1 \phi_1 = \left[\frac{\hbar^2}{2m^*} \nabla_1^2 + eV(r_1) + \int \frac{e^2}{4\pi\varepsilon} \frac{1}{r_{12}} |\phi_2(r_2)|^2 d^2 r_2 \right] \phi_1,$$
(9a)

$$E_2 \phi_2 = \left[\frac{\hbar^2}{2m^*} \nabla_2^2 + eV(r_2) + \int \frac{e^2}{4\pi\varepsilon} \frac{1}{r_{12}} |\phi_1(r_1)|^2 d^2 r_1 \right] \phi_2,$$
(9b)

where $\phi_1(r_1)$ and $\phi_2(r_2)$ are eigenstates of Eqs. (9a) and (9b). The calculation begins with solving the Poisson equation assuming no charge in the QD followed by a sequence of steps: solving the coupled Schrödinger equations for each electron; calculating the Coulomb interactions between the two electrons according to the third term of Eqs. (9a) and (9b); and recalculating the coupled Schrödinger equations if the eigenvalue is not converged. Using the obtained wave functions to calculate the new charge-density distributions, the 3D Poisson problem was solved again to obtain the confinement potential. Hence a new loop starts and the process will continue until the eigenvalue is converged. In practice, to ensure convergence, instead of the full new charge distribution ρ_n from the Schrödinger equation, a "damped" value, $\rho_{n+1} = \rho_n \eta + \rho_{n-1}(1-\eta)$, was used. Here ρ_{n-1} is the charge value acquired in the previous iteration. A small η reduces the risk of instability at the expense of more iterations to reach convergence.

The exchange energy, E_{ex}, was calculated according to

$$E_{ex} = \frac{e^2}{4\pi\varepsilon} \iint \phi_1(r_1) \phi_2(r_2) \frac{1}{r_{12}} \phi_1(r_2) \phi_2(r_1) d^2 r_1 d^2 r_2.$$
(10)

To validate our model, E_{ex} as a function of interdot distance was calculated at the same conditions as in Ref. 17 for two electrons in a double dot defined by an analytical potential. Results of both an exact numerical calculation and several approximation methods were included in Ref. 17. Fairly good agreement has been achieved between our model and Ref. 17 (not shown here). The deviation only becomes obvious when the interdot distance approaches zero (in this case it is practically a single dot).

Following the antisymmetry requirement of total electron wave functions (combined by orbital and spin part), the electron wave functions of the ground state can be constructed as $\psi(r_1, r_2) = \phi_1(r_1)\phi_2(r_2) + \phi_1(r_2)\phi_2(r_1)$. The charge-density distribution of the two-electron QD can be calculated according to

$$\rho_{(r_1)} = \int \psi^*(r_1, r_2) \psi(r_1, r_2) d^2 r_2$$

$$= \int |\phi_1(r_1)\phi_2(r_2) + \phi_1(r_2)\phi_2(r_1)|^2 d^2 r_2$$

$$= |\phi_1(r_1)|^2 + |\phi_2(r_1)|^2$$

$$+ 2\phi_1(r_1)\phi_2(r_1) \int \phi_2(r_2)\phi_1(r_2) d^2 r_2.$$
(11)

The calculated charge-density profile is superimposed onto the layout of the device in Fig. 4(d). The wave function of the formed dot is partially extended under the plunger gate which is kept at a close-to-zero bias. The Coulomb interactions push the two electrons far apart to form an elongated double quantum dot. A resulting exchange energy as low as a few μeV can be obtained.

V. MASTER EQUATION AND ITS INTERPRETATION TO EXPERIMENT

The model for describing the single-electron tunneling through the singlet-triplet (S-T) states, which are within the thermal fluctuation window kT, is plotted in Fig. 4(b). The tunneling through S-T states has notably different tunneling rates that can be experimentally determined as in Fig. 2(d). It is reasonable to assume that the tunneling through the triplet state S_+ has a much higher rate since the lower-energy singlet state S_- needs more thermal activation for tunneling to the partially occupied left lead. Now $|p, t\rangle = (p_1, p_+, p_-)'$; here p_- and p_+ are the occupation probability of the two-electron singlet state S_- and triplet state S_+, respectively; and p_1 is the occupation probability for the singly occupied state S_1 shown in Fig. 4(a).

The L matrix, along with the counting factor, is now given by

$$\begin{pmatrix} \Gamma_{in}^+ + \Gamma_{in}^- & -\Gamma_{out}^+ \cdot e^{i\chi} & -\Gamma_{out}^- \cdot e^{i\chi} \\ -\Gamma_{in}^+ & \Gamma_{out}^+ + \Gamma_{\mp} & \Gamma_{\pm} \\ -\Gamma_{in}^- & \Gamma_{\mp} & \Gamma_{out}^- + \Gamma_{\pm} \end{pmatrix}.$$
(12)

Here $\Gamma_{in}^\pm$ and $\Gamma_{out}^\pm$ are tunneling rate expressed by Eq. (1). $\Gamma_{\pm}$ and $\Gamma_{\mp}$ are the S-T transition rates governed by the detailed balance condition, $\Gamma_{\pm}/\Gamma_{\mp} = exp[(\mu_+ - \mu_-)/k_B T]$, where μ_+ and μ_- are the chemical potentials of the two states, respectively. The relaxation rate between S-T states is $1/T_1 = \Gamma_{\pm} + \Gamma_{\mp}$.

The calculation based on the above model shows reasonable agreement with the experimental data as plotted in Figs. 4(e) and 4(f). The theory describes both the significant enhancement of the shot noise and the large asymmetry of the distribution function and hence a negative $\frac{m_3}{m_1}$ at high tunneling rates. When the lower tunneling rate, within the kT window, is increased to be comparable with $1/T_1$, the slow state starts to contribute to transport noticeably. Consequently the distribution function will get more counts toward low elec-

tron numbers, resulting in a negative $\frac{m_3}{m_1}$. In the calculation we used a typical energy spacing of 15 μeV for the elongated QD, obtained from the self-consistent calculation; a long $T_1 = 10$ ms which is typical for a small S-T spacing;[18] and assuming $\Gamma_+ / \Gamma_- = 10$. Our observation and explanation is consistent with the notion that transport via a multilevel QD can enhance quantum noise.[11] The excess shot noise often observed in a large QD is due to the superposition of independent Poissonian processes of different levels with different sizes as explained in Ref. 11. The effect of bunching which was observed in a QD at nonequilibrium conditions was also attributed to possible multiple orbital states.[4] Our experiment clearly shows an a controllable evolution of the FCS from sub- to super-Poissonian of single-electron tunnelings in a two-level elongated double QD.

VI. CONCLUSIONS

By altering the tunneling rate, the FCS of real-time electron tunneling through a QD with its energy level aligned with one of its lead reservoirs reveals the noise tunability from sub- to super-Poissonian accompanied by a sign reversal of its third moment. A master-equation modeled transport through the spin singlet and triplet state of an elongated double dot allows us to explain the experimental findings consistently.

ACKNOWLEDGMENTS

[1] C. W. Gardiner and P. Zoller, *Quantum Noise*, Springer Series in Synergetics (Springer-Verlag, Berlin Heidelberg, 2004).

[2] K. MacLean, S. Amasha, I. P. Radu, D. M. Zumbuhl, M. A. Kastner, M. P. Hanson, and A. C. Gossard, Phys. Rev. Lett. **98**, 036802 (2007).

[3] T. Fujisawa, T. Hayashi, R. Tomita, and Y. Hirayama, Science **312**, 1634 (2006).

[4] S. Gustavsson, R. Leturcq, B. Simovič, R. Schleser, P. Studerus, T. Ihn, K. Ensslin, D. C. Driscoll, and A. C. Gossard, Phys. Rev. B **74**, 195305 (2006).

[5] S. Gustavsson, R. Leturcq, B. Simovič, R. Schleser, T. Ihn, P. Studerus, K. Ensslin, D. C. Driscoll, and A. C. Gossard, Phys. Rev. Lett. **96**, 076605 (2006).

[6] Leonid S. Levitov, Hyunwoo Lee, and Gordey B. Lesovik, J. Math. Phys. **37**, 4845 (1996).

[7] D. A. Bagrets and Yu. V. Nazarov, Phys. Rev. B **67**, 085316 (2003).

[8] L. M. K. Vandersypen, J. M. Elzerman, R. N. Schouten, L. H. Willems van Beveren, R. Hanson, and L. P. Kouwenhoven, Appl. Phys. Lett. **85**, 4394 (2004).

[9] J. M. Elzerman, R. Hanson, J. S. Greidanus, L. H. Willems van Beveren, S. De Franceschi, L. M. K. Vandersypen, S. Tarucha, and L. P. Kouwenhoven, Phys. Rev. B **67**, 161308(R) (2003).

[10] W. Lu, Z. Ji, L. Pfeiffer, K. W. West, and A. J. Rimberg, Nature (London) **423**, 422 (2003).

[11] W. Belzig, Phys. Rev. B **71**, 161301(R) (2005).

[12] M. Ciorga, A. S. Sachrajda, P. Hawrylak, C. Gould, P. Zawadzki, S. Jullian, Y. Feng, and Z. Wasilewski, Phys. Rev. B **61**, R16315 (2000).

[13] M. C. Rogge, B. Harke, C. Fricke, F. Hohls, M. Reinwald, W. Wegscheider, and R. J. Haug, Phys. Rev. B **72**, 233402 (2005).

[14] D. H. Cobden and B. A. Muzykantskii, Phys. Rev. Lett. **75**, 4274 (1995).

[15] I.-H. Tan, G. L. Snider, D. L. Chang, and E. L. Hu, J. Appl. Phys. **68**, 4071 (1990).

[16] Y. W. Suen, J. Jo, M. B. Santos, L. W. Engel, S. W. Hwang, and M. Shayegan, Phys. Rev. B **44**, 5947 (1991).

[17] J. Pedersen, C. Flindt, N. A. Mortensen, and A. P. Jauho, Phys. Rev. B **76**, 125323 (2007).

[18] R. Hanson, L. P. Kouwenhoven, J. R. Petta, S. Tarucha, and L. M. K. Vandersypen, Rev. Mod. Phys. **79**, 1217 (2007).